

# Decaying quantum turbulence in a two-dimensional Bose-Einstein condensate at finite temperature

Andrew J. Groszek<sup>1, 2\*</sup>, Matthew J. Davis<sup>3</sup>, Tapio P. Simula<sup>2, 4</sup>

**1** Joint Quantum Centre (JQC) Durham–Newcastle, School of Mathematics, Statistics and Physics, Newcastle University, Newcastle upon Tyne NE1 7RU, United Kingdom

**2** School of Physics and Astronomy, Monash University, Victoria 3800, Australia

**3** ARC Centre of Excellence in Future Low-Energy Electronics Technologies, School of Mathematics and Physics, University of Queensland, Brisbane, Queensland 4072, Australia

**4** Centre for Quantum and Optical Science, Swinburne University of Technology, Melbourne 3122, Australia

\* andrew.groszek@newcastle.ac.uk

December 20, 2024

## Abstract

We numerically model decaying quantum turbulence in two-dimensional disk-shaped Bose–Einstein condensates, and investigate the effects of finite temperature on the turbulent dynamics. We prepare initial states with a range of *condensate temperatures*, and imprint equal numbers of vortices and antivortices at randomly chosen positions throughout the fluid. The initial states are then subjected to unitary time-evolution within the c-field methodology. For the lowest condensate temperatures, the results of the zero temperature Gross–Pitaevskii theory are reproduced, whereby vortex evaporative heating leads to the formation of Onsager vortex clusters characterised by a negative absolute *vortex temperature*. At higher condensate temperatures the dissipative effects due to vortex–phonon interactions tend to drive the vortex gas towards positive vortex temperatures dominated by the presence of vortex dipoles. We associate these two behaviours with the system evolving toward an anomalous non-thermal fixed point, or a Gaussian thermal fixed point, respectively. The cross-over between these two dynamical behaviours is found to occur at earlier times with increasing condensate temperature.

---

## Contents

<b>1</b>	<b>Introduction</b>	<b>2</b>
<b>2</b>	<b>C-field modelling of finite temperature Bose-Einstein condensates</b>	<b>3</b>
2.1	Initial state preparation	3
2.2	Microcanonical evolution	5
2.3	Numerical details	5
<b>3</b>	<b>Results</b>	<b>5</b>
3.1	Evaporative heating of vortices	5
3.2	Vortex thermometry	6
3.3	Vortex number decay	8

3.4	Evolution toward an anomalous non-thermal fixed point	8
<b>4</b>	<b>Conclusions and outlook</b>	<b>11</b>
	<b>References</b>	<b>13</b>

---

## 1 Introduction

Developing a complete understanding of turbulent dynamics in fluids remains a significant challenge in contemporary physics. Over many decades of research, a wide range of emergent features have been identified in turbulent systems, such as cascades of energy and enstrophy through wavenumber space [1–3]. However, in general such features have proven highly nontrivial to describe from first principles. Recently, quantum turbulence (QT) in superfluids has emerged as a mature research field [4], and is promising insights into many long-standing problems of hydrodynamics [5]. On a microscopic level, the structure of QT is fundamentally different from its classical counterpart, taking the form of a tangled network of quantised, topologically protected vortex filaments. Nonetheless, many results from classical hydrodynamics have already been reproduced in superfluid systems [6–8], including the Kolmogorov  $k^{-5/3}$  energy scaling law [9, 10].

In the case of two-dimensional (2D) turbulence, this classical–quantum connection has motivated several studies aimed at realising the inverse energy cascade in 2D QT [11–16]—a well known phenomenon in driven classical 2D turbulence [2, 17]. In 2D superfluid turbulence this phenomenon, as predicted by Onsager’s thermodynamic model of point-like vortices [18], should be associated with the clustering of same-sign vortices at negative absolute vortex temperatures [13, 15, 19–23]. Indeed, the applicability of Onsager’s model to 2D QT is striking—in two recent experiments [24, 25], large numbers of vortices were injected into planar Bose–Einstein condensates (BECs) and evidence was obtained for the formation of high-energy Onsager vortex clusters. These experiments have only become possible recently due to advances in the imaging and control of quasi-2D BECs [26, 27], as well as the possibility of detecting vortex signs in a turbulent state [28, 29].

Previous numerical work on the dynamics of randomly imprinted vortices in planar BECs identified that Onsager vortices could emerge in the ensuing dynamics, using both a Gross–Pitaevskii model and a 2D point vortex model with phenomenological pair annihilation [20]. The mechanism for the Onsager vortex formation was identified as being evaporative heating, where vortex pair annihilation led to an increased energy per vortex, and forced the system into the negative absolute temperature region of the vortex phase space. Subsequent analysis showed that Onsager vortex formation was inhibited in harmonically trapped BECs due to the inhomogeneous condensate density [21]. The same authors also found that the inclusion of phenomenological dissipation representing the effects of damping due to finite condensate temperature also had a deleterious effect on the formation of Onsager vortices [21]. These findings raised important questions regarding the possibility of experimentally observing Onsager vortices in decaying two-dimensional quantum turbulence, and motivate more quantitative studies of the effect of the temperature of the atoms in these systems.

Here we revisit the question of how non-zero condensate temperature affects Onsager vortex formation in decaying two-dimensional quantum turbulence. Rather than incorporating thermal atom effects in the GPE using a phenomenological damping term, we instead perform dynamical simulations using

the classical field methodology [30–32]. The unitary projected Gross–Pitaevskii equation (PGPE) that conserves both the energy and the normalisation of the classical field is used for describing the dynamics of the Bose gas. We systematically vary the initial condensate temperature by sampling microstates using the stochastic projected Gross–Pitaevskii equation (SPGPE) [32, 33], and determine the resulting effect on the turbulent dynamics for an ensemble of statistically equivalent vortex distributions. We focus on low temperature finite-size systems in which thermal activation of vortex-antivortex pairs is suppressed [34]. We quantify the dynamics using the vortex thermometry methodology [23] facilitated by vortex classification techniques [13, 35]. Our results show that for sufficiently cold condensates, there is little difference from the predictions of the zero temperature GPE. Furthermore, our results suggest that the vortex evaporative heating mechanism overwhelms the dissipative effects due to thermal atoms for condensate fractions above approximately 80% for our model, which is an experimentally attainable regime.

This paper is organised as follows: in Section 2 we give a brief overview of the c-field methodology, including the initial state preparation at finite temperature and the numerical techniques employed. Section 3 presents the numerical results for the decaying quantum turbulence at finite temperature, and uses vortex thermometry to analyse the dynamics of the vortex subsystem. The time-dependence of the nearest-neighbour vortex spacing provides evidence of a cross-over from evolution towards an anomalous non-thermal fixed point to a thermal fixed point. Finally, we discuss the results and conclude in Section 4.

## 2 C-field modelling of finite temperature Bose-Einstein condensates

In this work we model the dynamics of a partially-condensed Bose gas at finite temperature using a projected [31, 32, 36] and stochastic projected [32, 33, 37] Gross–Pitaevskii equation. Our numerical modelling consists of two distinct stages. We first prepare a number of statistically equivalent initial conditions for the Bose field confined by a two-dimensional disk trap at a given condensate temperature, varying both the spatial noise distribution (generated by evolving the SPGPE) and the initial vortex configuration (randomly imprinted into the field) for each state. We then perform microcanonical evolution for each of the initial states using the energy conserving PGPE. We outline these steps in detail below.

### 2.1 Initial state preparation

We begin by finding the ground state of the trapping potential,  $V_{\text{tr}}(\mathbf{r})$ , using imaginary time propagation of the zero-temperature projected Gross–Pitaevskii equation,

$$i\hbar \frac{\partial \psi(\mathbf{r}, t)}{\partial t} = \mathcal{P}\{L_{\text{GP}}\psi(\mathbf{r}, t)\}. \quad (1)$$

Here  $\psi(\mathbf{r}, t)$  is the classical Bose field that includes only the highly-occupied, low momentum modes of the gas below a chosen cutoff. The Gross-Pitaevskii operator is

$$L_{\text{GP}} = -\frac{\hbar^2}{2m} \nabla_{2\text{D}}^2 + V_{\text{tr}}(\mathbf{r}) + g|\psi(\mathbf{r}, t)|^2, \quad (2)$$

where  $m$  is the atomic mass, and  $g = 4\pi\hbar^2 a_s N/ml_z$  is the two-dimensional interaction constant describing the strength of the  $s$ -wave interatomic collisions (with scattering length  $a_s$ ) for system with (uniform) axial extent  $l_z$  and total atom number  $N$ . The projection operator  $\mathcal{P}$  ensures that no population

is transferred to the higher momentum modes in the numerics. From here on, the time dependence of the classical field is implied,  $\psi(\mathbf{r}) \equiv \psi(\mathbf{r}, t)$ .

To numerically represent a uniform disk geometry, we use a potential  $V_{\text{tr}}(r) = \mu_o(r/R)^{30}$  with trap radius  $R \approx 60 \xi_o$ , where  $\mu_o$  is the chemical potential of the ground state, and  $\xi_o = \hbar/(2m\mu_o)^{1/2}$  is the corresponding healing length (which is on the order of the vortex core size). We set  $g = 5250 \hbar^2/m$ , which for a gas of  $10^{5-87}$  Rb atoms would correspond to a cloud with  $l_z \approx 1.3 \mu\text{m}$ . Throughout this work, we adopt units of  $\mu_o$  (energy),  $\xi_o$  (length),  $t_o \equiv \hbar/\mu_o$  (time) and  $T_o \equiv 10^{-5} \mu_o/k_B$  (fluid temperature).

The effects of finite condensate temperature are incorporated by subsequently evolving the classical Bose field using the stochastic projected Gross–Pitaevskii equation. This is a grand canonical theory, where the high energy single-particle modes are treated as a thermalised reservoir, with well-defined temperature  $T$  and chemical potential  $\mu$ , that exchanges particles and energy with the classical field [32]. In Stratonovich form, the SPGPE is expressed as:

$$d\psi(\mathbf{r}) = \mathcal{P} \left\{ -\frac{i}{\hbar} L_{\text{GP}} \psi(\mathbf{r}) dt + \frac{\gamma}{\hbar} (\mu - L_{\text{GP}}) \psi(\mathbf{r}) dt + dW(\mathbf{r}, t) \right\}, \quad (3)$$

where  $\gamma$  is a dimensionless growth coefficient, and the complex noise term  $dW(\mathbf{r}, t)$  is spatially and temporally uncorrelated, with its only nonzero moment given by  $\langle dW^*(\mathbf{r}, t) dW(\mathbf{r}', t) \rangle = (2\gamma k_B T dt / \hbar) \delta(\mathbf{r} - \mathbf{r}')$ . The first term on the right hand side of Eq. (3) corresponds to unitary evolution of the field, while the second and third terms model condensate growth processes resulting from collisions of atoms above the momentum cutoff enforced by  $\mathcal{P}$  [32, 33, 37].

To generate a thermalised classical field at a chosen temperature  $T$ , we evolve the SPGPE using a damping parameter of  $\gamma = 10^{-2}$  (although this choice is arbitrary and does not affect the final equilibrium state). The reservoir chemical potential is chosen to be  $\mu = \mu_o$ , and the temperature is set to a constant value in the range  $0 < T/T_o \lesssim 3$  throughout each simulation. For comparison, the critical temperature for condensation in this system is  $T_c \approx 10 T_o$  which we find by estimating the temperature at which the condensate fraction vanishes in equilibrium (see below for details regarding the condensate fraction measurement).

After an initial burn-in time of  $\sim 200 t_o$ , the norm  $\int |\psi(\mathbf{r})|^2 d\mathbf{r} \approx 1$  (which is weakly temperature-dependent) and the total energy attain approximately stable values (with fluctuations  $\lesssim 1\%$ ), indicating that equilibrium has been reached. For each chosen temperature, 50 uncorrelated samples of the stochastically evolving field are used as thermalised initial conditions.

At a given temperature, the condensate fraction  $n_0$  can be extracted from a large number of uncorrelated states by applying the Penrose–Onsager criterion [38], whereby  $n_0$  is identified as the largest eigenvalue of the one-body density matrix,  $\rho(\mathbf{r}, \mathbf{r}') = \langle \psi^*(\mathbf{r}) \psi(\mathbf{r}') \rangle$ , with the average taken over different stochastic realisations. The condensate mode  $\psi_0(\mathbf{r})$  is then given by the corresponding eigenvector. For our chosen temperatures, the measured condensate fraction ranges between  $0.75 \lesssim n_0 \lesssim 1$ . When making comparisons with experiments it is important to keep in mind that these values are only an approximation to the true condensate fraction, as thermal atoms with momenta above the cutoff are not included in the classical field.

For each of the sampled initial conditions, vortices are then imprinted by multiplying the field  $\psi(\mathbf{r})$  by an ansatz function  $\eta(\mathbf{r})$ , which establishes both a density dip and a  $2\pi$  phase-winding around each chosen vortex core location. The ansatz is defined

$$\eta(\mathbf{r}) = \prod_{k=1}^{N_v} \chi(\mathbf{r} - \mathbf{r}_k) \exp \left[ i s_k \arctan \left( \frac{y - y_k}{x - x_k} \right) \right], \quad (4)$$

where  $N_v$  is the number of vortices being imprinted, and  $\mathbf{r}_k = (x_k, y_k)$  and  $s_k \in \pm 1$  are the position and sign, respectively, of the  $k$ th vortex. The real function  $\chi(\mathbf{r}) = r/(r^2 + 2\xi_o^2)^{1/2}$  captures the density profile

of each vortex core [39]. We imprint  $N_v = 100$  randomly distributed vortices, with equal numbers of each sign to ensure that the angular momentum of the condensate remains close to zero. After the vortices have been imprinted, the field is normalised to its initial value to avoid a net loss of probability density. The vortex imprinting adds a small amount of kinetic energy to the system and therefore slightly increases the temperature of the field.

## 2.2 Microcanonical evolution

After vortex imprinting, the turbulent dynamics are simulated by evolving each state using the PGPE for  $t \approx 5500 t_o$ . The phonons of the field interact with the vortices, causing additional damping and changing the nature of the decaying turbulence. During the evolution we track the positions of the vortices over time by locating phase singularities in the classical field. To avoid spurious vortex detections due to density fluctuations at high temperatures, we first coarse-grain the field by removing spatial frequencies beyond  $\pi/\xi_o$  before performing the vortex detection step. Additionally, we only count vortices within the region  $r < 0.95 R$ .

## 2.3 Numerical details

We represent the field on a numerical grid of size  $(512)^2$ , and perform temporal evolution using a fourth-order adaptive Runge–Kutta technique in the software package XMDS2 [40]. The spatial resolution is set such that the grid spacing  $\Delta x \approx \xi_o/3.5$ .

Numerically, we implement the projector  $\mathcal{P}$  in Fourier space, where it takes the form of a binary mask which has a value of unity for  $|\mathbf{k}| < k_{\text{cut}}$ , and is zero outside this region. This prevents occupation of any modes of  $\psi(\mathbf{r})$  beyond a wavenumber of  $k_{\text{cut}}$ . To ensure that the field is de-aliased, we set the cutoff for the projector to  $k_{\text{cut}} = k_{\text{max}}/2$ , where  $k_{\text{max}} = \pi/\Delta x$  is the largest wavenumber that can be represented on our numerical grid.

# 3 Results

## 3.1 Evaporative heating of vortices

Figure 1 shows exemplary simulation results of decaying two-dimensional quantum turbulence. Figure 1(a)–(c) are for a system at zero condensate temperature and condensate fraction  $n_0 = 1$ , and Fig. 1(d)–(e) are at finite temperature with a condensate fraction of  $n_0 \approx 0.75$ . Each frame (a)–(f) shows three snapshots (i–iii) from the simulated dynamics with time increasing from left to right. The top rows show the condensate density, with vortices visible as dark spots. The middle rows show the phase of the classical field, with the locations of vortices and antivortices denoted by black circles and white squares, respectively. The bottom rows show the vortices after they have been classified as same-sign clusters (blue/green markers), vortex dipoles (red markers) and free vortices (yellow markers) [13, 23, 35], as well as the streamlines of the incompressible velocity field of the condensate, which have been approximated using a point-vortex model [20, 41].

In Figure 1(a), a high frequency phonon field develops over time due to the vortex–sound interactions, although these density oscillations have low amplitude. By contrast, at higher condensate temperatures [panel (d)] the density fluctuations are much more prominent, and hence the visibility of the vortex cores is reduced significantly. The vortices are also observed to decay much faster at these temperatures due to the dissipative effect associated with the vortex–phonon interactions.

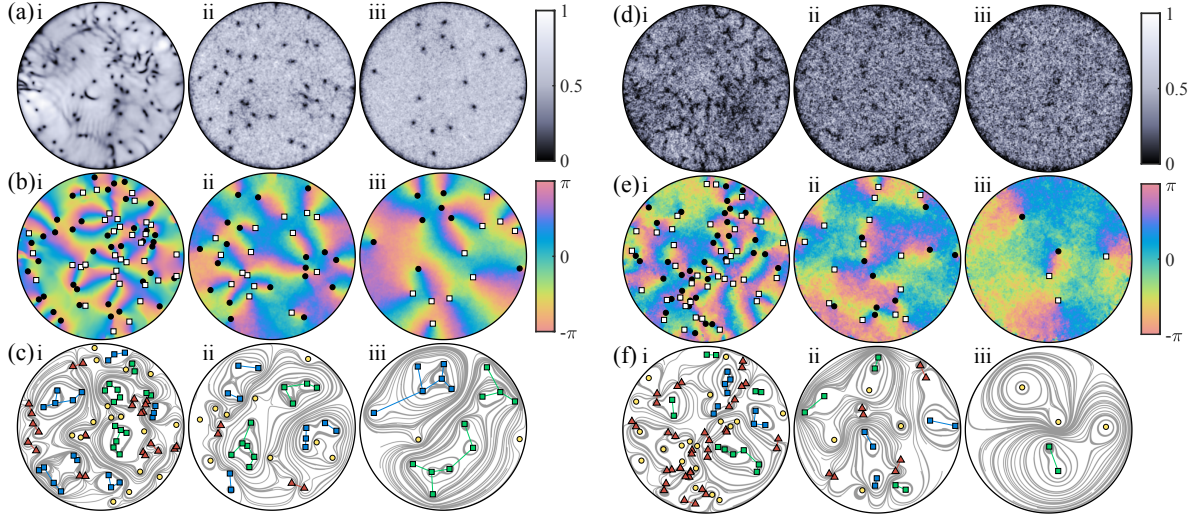


Figure 1: Temporal evolution of the classical field  $\psi(\mathbf{r})$  for two condensate fractions,  $n_0 = 1$  [(a)–(c)] and  $n_0 \approx 0.75$  [(d)–(f)], with frames i, ii and iii in each row corresponding to times  $t/t_0 \approx 10$ ,  $t/t_0 \approx 900$  and  $t/t_0 \approx 4500$ , respectively. For each case the classical field density  $|\psi(\mathbf{r})|^2$  is shown in rows (a) and (d), the phase in (b) and (e), and the classified vortices and incompressible velocity field streamlines in (c) and (f). In (b) and (e), vortices (antivortices) are indicated with black dots (white squares), while in (c) and (f), clusters of vortices (antivortices) are identified as blue (green) squares, dipoles as red triangles, and free vortices as yellow circles. In rows (a) and (d), the density is normalised to its maximum value,  $1.7 \times 10^{-4} \xi_0^{-2}$  and  $3.0 \times 10^{-4} \xi_0^{-2}$ , respectively.

In cold condensates (a)–(c) the vortex evaporative heating mechanism drives the vortex gas towards states with higher incompressible kinetic energy per vortex, resulting in the formation of Onsager vortex clusters [20, 21] [most evident in panel (c)iii]. In warmer condensates (d)–(f) the vortex cooling effect due to the dissipative interaction with the non-condensate atoms overwhelms the vortex evaporative heating mechanism, and hence the formation of Onsager vortex clusters is suppressed.

### 3.2 Vortex thermometry

In statistical equilibrium a 2D vortex gas can be described by a vortex temperature [18, 20, 23], which determines the energy of the flow field. In the uniform disk system considered here, there are three distinct equilibrium phases of the neutral vortex gas: (i) at low energies ( $\beta \gg 0$ ) the vortices arrange into dipole pairs, (ii) at intermediate energies ( $\beta \approx 0$ ) the vortices distribute themselves randomly throughout the system, and (iii) at the highest energies ( $\beta \ll 0$ ) the vortices arrange into two large clusters (one of each circulation sign)<sup>1</sup>. Here, we are able to extract this vortex temperature directly from our simulations by monitoring the fractional populations of classified vortex dipoles and clusters [35]. This is possible because these populations both vary monotonically with temperature in thermodynamic equilibrium, and thus can be used as thermometers as shown previously by Groszek *et al.* [23].

In Fig. 2, the fractional populations of vortices belonging to (a) vortex clusters and (b) vortex dipoles are shown as a function of time, in addition to (c) the inverse vortex temperature  $\beta$  extracted from the clustered fraction [23]. At zero condensate temperature, the clustered fraction grows fairly

<sup>1</sup>The negative absolute temperatures corresponding to the highest energies are the result of the bounded phase space of the vortex system [18].

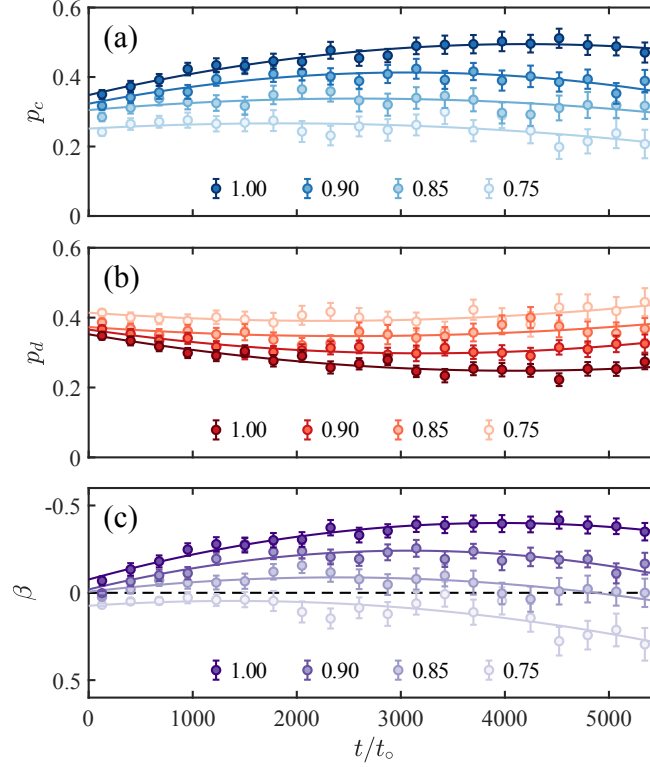


Figure 2: Fractional population curves of (a) vortex clusters and (b) vortex dipoles, as well as (c) the resulting inverse vortex temperature  $\beta$ , measured using the cluster population [23]. All data points have been ensemble averaged over 50 stochastic realisations, as well as temporally binned, and the error bars correspond to the standard error in the mean of each measurement. The legend in each subfigure indicates the condensate fraction, and the solid lines shown are quadratic fits to the data, serving as a guide to the eye.

monotonically as the vortex gas evaporatively heats up [panel (a)], while the dipole fraction decays correspondingly [panel (b)]. These trends indicate that the vortex gas is evolving towards states with higher energy per vortex [20]. By contrast, at the highest condensate temperature ( $n_0 \approx 0.75$ ), the clustered (dipole) fraction shows a decreasing (increasing) trend, corresponding to a more rapid loss of incompressible kinetic energy over time.

For all condensate fractions the vortex temperature [Fig. 2(c)] begins near  $\beta = 0$ , and shows evidence of initial evaporative heating of vortices (towards negative  $\beta$ ). However, in all cases, there is a turning point at which the gradient of  $\beta(t)$  changes sign and the vortex system begins to cool. The timescale at which this occurs decreases with increasing condensate temperature, indicating that the dissipation of vortex energy into sound becomes increasingly strong as the initial condensate temperature is increased. Note that, in this figure, positive temperatures are scaled with respect to the Berezinskii–Kosterlitz–Thouless transition temperature [42–45],  $\beta_{\text{BKT}} = E_o/2$ , while the negative temperatures are expressed in terms of the Einstein–Bose vortex condensation temperature [35, 42, 46],  $\beta_{\text{EBC}} = N_v E_o/4$ , where the constant  $E_o = \rho_s \kappa^2/4\pi$  is defined in terms of the superfluid density  $\rho_s$  and the quantum of circulation  $\kappa = h/m$ .

### 3.3 Vortex number decay

As the fluid (vortex–phonon system) relaxes toward equilibrium, the number of vortices,  $N_v(t)$ , gradually decays due to vortex–antivortex annihilations—mostly within the bulk of the condensate, but occasionally also at the boundary [21]. This number decay behaviour has been a topic of recent interest [21, 47–53] and several attempts have made to describe the decay process using phenomenological rate equations. A consensus seems to be developing that three-vortex (or even four-vortex) events significantly affect the observed dynamics [21, 51–53]; however, the precise form of the rate equation is still a topic of debate.

We have previously proposed a vortex number decay law of the form [21]

$$\frac{dN_v}{dt} = -\Gamma_1 N_v - \Gamma_2 N_v^2 - \Gamma_3 N_v^3 - \Gamma_4 N_v^4, \quad (5)$$

where each  $\Gamma_n$  term on the right hand side of the equation is interpreted as an  $n$ -body decay rate—i.e. the rate at which  $n$  vortices will collide and lead to an annihilation event (of at least two of those vortices). In this interpretation,  $\Gamma_1$  is the rate at which vortices leave via the boundary, as single-vortex loss is topologically prohibited in the fluid bulk.

Karl and Gasenzer [52] recently suggested that the decay should instead be modelled using

$$\frac{dN_v}{dt} = -\Gamma_2 N_v^2 - \Gamma_3 N_v^{7/2}, \quad (6)$$

where the extra factor of  $N_v^{1/2}$  in the three-body term accounts for the vortex-density–dependent velocity of the vortices, which should affect the probability of three-vortex encounters. The one-body term was omitted in their model as their calculations involved an unbounded fluid.

In Fig. 3, we present the measured vortex numbers  $N_v$  as functions of reduced time  $t/t_o$  (solid green lines) for the four different condensate fractions. When fitting the two rate equations (5) and (6), we find that both describe the data equally well. However, since the latter involves fewer free parameters, we opt to use it over our earlier model. The resulting fits are shown as dashed lines in Fig. 3, and the corresponding values of the two fitting parameters are shown as a function of condensate temperature in the insets. Physically, Eq. (6) supports the interpretation that three-body annihilations are significantly more frequent than four-body events, as had been previously argued in Ref. [21]. If the observed  $\Gamma_3(T)$  trend were to continue, our data suggest that the three-body term should become negligible at  $T \sim 6 T_o$ , and lower-order terms would dominate. We note that a one-body term would eventually have to be added to the model at higher condensate temperatures to describe the increasingly steep  $N_v(t)$  gradient.

An additional complicating factor in interpreting the physics captured by these phenomenological rate equations arises due to the fact that the decay ‘constants’  $\Gamma_n(N_v(t))$  are actually time-dependent, as the dominant microscopic decay dynamics are drastically different depending on the density and configuration of the vortex system. It is therefore desirable to find alternative and complementary ways of describing the statistical evolution of the vortices.

### 3.4 Evolution toward an anomalous non-thermal fixed point

A successful approach to understanding systems far from equilibrium in general, and 2D QT in particular, has been to characterise them using stable statistical distributions that are only weakly dependent on microscopic details of the system, which may themselves vary in time. An important example is the discovery of non-thermal fixed points and their characterisation in terms of far from equilibrium universality classes [54, 55].

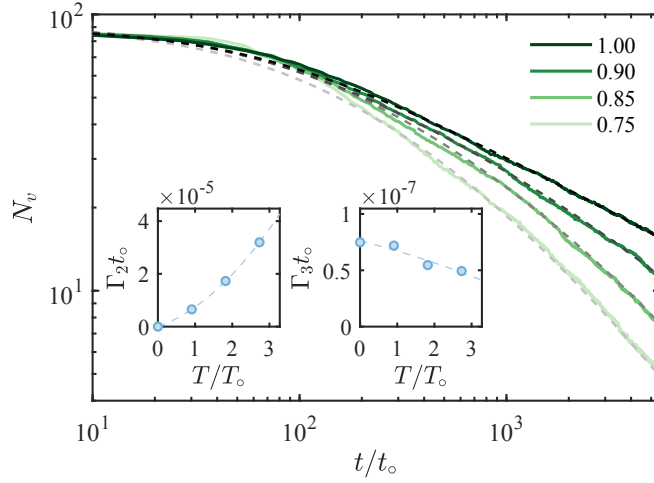


Figure 3: Ensemble averaged vortex number decay curves for all four condensate temperatures (solid green lines), with fits to Eq. (6) (dashed grey lines). The insets show the measured decay constants as functions of the reduced temperature, with quadratic fits (dashed lines) included as a guide to the data.

Previously, Groszek *et al.* [23] identified related scale invariant behaviour by expressing the populations of vortex clusters and dipoles in terms of the total number of vortices remaining in the system, effectively removing the time dependence inherent to the vortex number decay. This analysis revealed that the decaying quantum turbulence rapidly approaches a quasiequilibrium steady state characterised by the emergence of power-law distributions. In such a state, it was argued that the vortices must have enough time between each annihilation event to rearrange themselves into the maximum entropy configuration available at their energy. Hence, there are two relevant rates that determine whether the vortex gas has reached quasiequilibrium. The first is the rate at which vortex–antivortex annihilation events are occurring, defined at a given time as

$$v_{\text{ann}} \equiv \frac{1}{2} \frac{dN_v}{dt}, \quad (7)$$

where the factor of one-half accounts for the two vortices lost per annihilation. The second is the rate at which the vortices reconfigure themselves, which we approximate as the inverse of the mean time it takes for a vortex to travel the distance to its nearest neighbour, i.e.  $v_{ij} \approx \bar{u}/d_{ij}$ . Here,  $\bar{u} \approx (\hbar/m)(1/d_{ij})$  is the mean velocity of a vortex in a configuration with mean intervortex spacing  $d_{ij} \approx R/N_v^{1/2}$ . Hence,

$$v_{ij} \approx \frac{\hbar N_v}{mR^2}. \quad (8)$$

When  $v_{\text{ann}} < v_{ij}$ , the annihilations should be infrequent enough for the system to reach the aforementioned steady state. The two rates can be measured directly from the  $N_v(t)$  curves in Fig. 3, and we compare the results in Fig. 4(a) for each initial condensate temperature as a function of vortex number<sup>2</sup>. The point at which quasiequilibrium is reached in each case is indicated with a grey dot.

Figure 4(b) shows the measured cluster  $N_c$  and dipole  $N_d$  populations as functions of the total vortex number  $N_v$  in the system for the four initial condensate temperatures, where the curves have

<sup>2</sup>Note that we have calculated  $v_{\text{ann}}$  using the fits to Eq. (6), rather than the raw  $N_v(t)$  data, in order to eliminate noise arising from numerical differentiation.

been vertically offset for clarity. Once the state of quasiequilibrium has been reached, the curves are well approximated as power-laws, as seen previously [23]. The exponents at zero temperature are

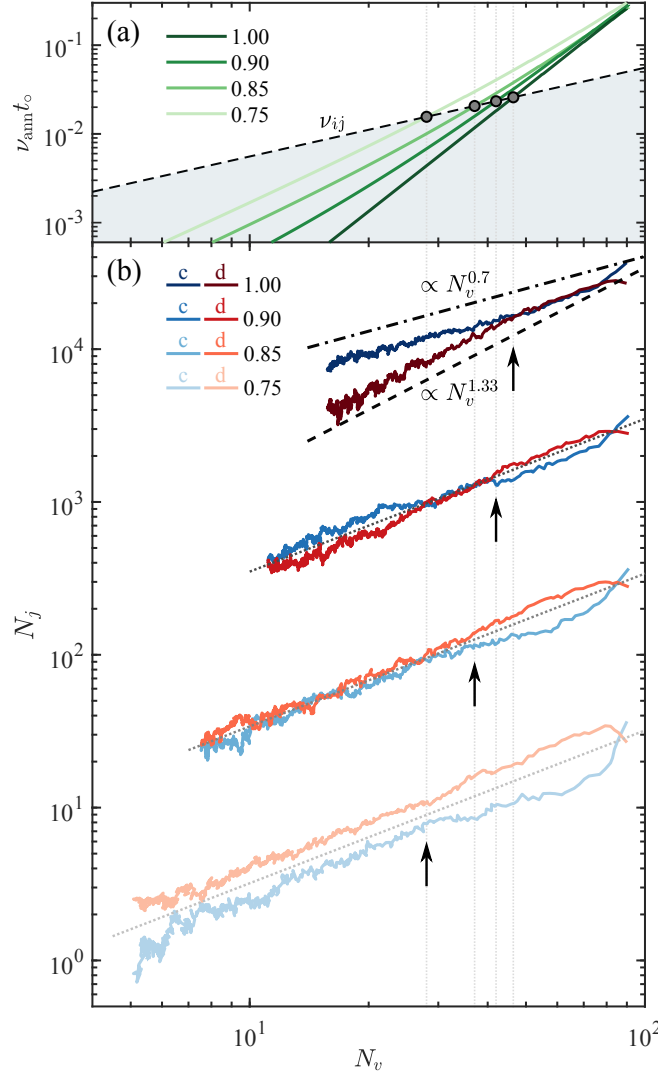


Figure 4: (a) The vortex annihilation rates  $v_{\text{ann}}$  for all four initial condensate temperatures (solid green lines) are compared to the rate  $v_{ij}$  of vortex reconfiguration (dashed line) as a function of the total vortex number. The shaded region indicates quasiequilibrium, where  $v_{\text{ann}} < v_{ij}$ , and the black dots denote the points at which this condition is first met for each condensate temperature. (b) The mean number of vortex clusters ( $j = c$ , blue) and vortex dipoles ( $j = d$ , red) as functions of total vortex number  $N_v$  for each initial condensate temperature. For clarity, the curves are shifted vertically by multiplying  $N_j$  by  $10^n$ , where  $n = \{0, 1, 2, 3\}$  for  $n_0 = \{0.75, 0.85, 0.90, 1.00\}$ , respectively. For  $n_0 = 1.00$ , the data compare well with  $N_c \sim N_v^{0.7}$  (dot-dashed line) and  $N_d \sim N_v^{1.33}$  (dashed line). For all other temperatures,  $N_j \sim N_v$  (dotted lines) yields a more reasonable comparison. The vertical dotted grey lines are traced from the quasiequilibration points identified in panel (a), and these points are highlighted on each appropriate  $N_j$  curve by vertical arrows. Note that time flows right to left in this figure.

consistent with  $N_c \sim N_v^{0.7}$  (dot-dashed line) and  $N_d \sim N_v^{1.33}$  (dashed line), while at the other condensate temperatures  $N_c \sim N_d \sim N_v$  (dotted lines). All four cases show a clear distinction between early- and late-time behaviour, with the cross-over aligning well with the time at which  $v_{\text{ann}} = v_{ij}$  (see the arrows in the figure). At early times (high vortex density), the number of dipoles is always greater than or equal to the number of clusters, before the decay transitions to the late time behaviour, which depends strongly on the fluid temperature. There is also a very early cross-over from cluster-dominated to dipole-dominated behaviour (at  $N_v \approx 90$  in each case), which results from the quench-like initial condition. These curves are suggestive of the interpretation that in the limit of vanishing total vortex number ( $N_v \rightarrow 0$ ), the ultimate fate of the vortex system would be 100% clusters in the two coldest condensate temperature systems and 100% dipoles in the two hottest condensate temperature systems (assuming no further changes to the statistical behaviour would occur).

These two final states act as attractors for the turbulent evolution, and can be interpreted as fixed points at which the dynamics of the system critically slow down, and universal scaling laws emerge [56, 57]. In the case where the system becomes dipole-dominated, the attractor is a Gaussian fixed point, which corresponds to a state where all vortices have annihilated and the fluid thermalises. By contrast, when the vortices form same-sign clusters, annihilation events become infrequent, and the system becomes ‘stuck’ in a non-equilibrium configuration for an extended period of time. Such behaviour corresponds to an anomalous non-thermal fixed point. It is predicted that the system would eventually return to the Gaussian fixed point; although the time required to do so may approach infinity as  $T \rightarrow 0$ .

Karl and Gasenzer [52] recently demonstrated that the evolution towards each of these attractors can be related to the vortex distributions through the theory of phase-ordering kinetics. They found that, if the system is evolving towards the non-thermal fixed point, the mean nearest-neighbour vortex distance should scale as  $d_{\text{nn}} \sim t^{1/5}$ . By contrast, as the system approaches the Gaussian fixed point, the scaling should instead have the form  $d_{\text{nn}} \sim t^{1/2}$ . Here, we measure  $d_{\text{nn}} \equiv \sum_j \min_{k \neq j} |\mathbf{r}_k - \mathbf{r}_j| / N_v$  for all four condensate temperatures, and present the results as a function of time in Fig. 5.

While the two coldest temperatures show scaling close to the  $\sim t^{1/5}$  prediction for the anomalous non-thermal fixed point, the hottest temperature shows no evidence of this, instead approaching the  $\sim t^{1/2}$  prediction at late times, which should correspond to evolution towards the thermal fixed point. The  $n_0 = 0.85$  condensate fraction case appears to transition between the two behaviours, suggesting that the dynamics undergo a cross-over between the two trajectories. These observations are consistent with the expected behaviour: the evaporative heating mechanism drives the system towards non-thermal fixed points, whereas the dissipative vortex–phonon interactions drive the system toward thermalisation.

## 4 Conclusions and outlook

Here we have studied decaying two-dimensional quantum turbulence in Bose–Einstein condensates at finite temperatures using a classical field approach. As is the case with simpler phenomenologically damped mean-field models, the non-condensate fraction has a strong influence on the vortex dynamics. Microscopically, the non-condensate atom density modifies the condensate density in the vicinity of the vortices, and this density modulation results in a Magnus force with a component along the direction of the motion of a vortex [58, 59]. For an isolated vortex–antivortex dipole, this force component causes the pair to move closer to each other, eventually leading to their annihilation. At zero condensate temperature the Magnus force remains orthogonal to the vortex velocity vector, and therefore isolated vortex–antivortex pairs cannot annihilate. The energetics of the decaying vortex system are driven by

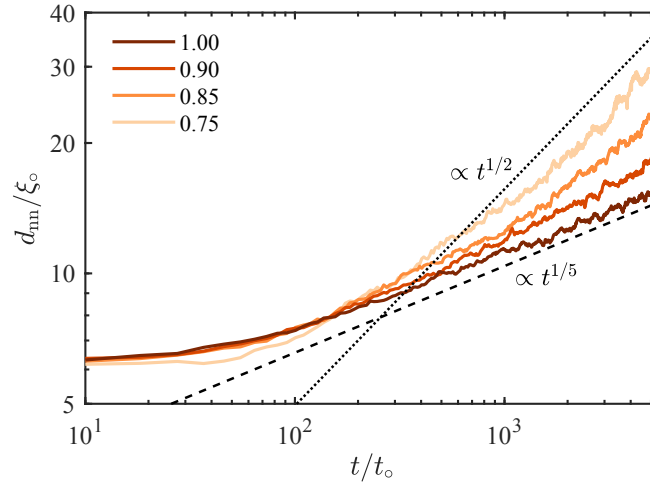


Figure 5: Mean nearest-neighbour vortex distance  $d_{nn}$  as a function of time for all four initial condensate temperatures. The power-laws corresponding to the two fixed points, discussed in Ref. [52], are shown as dashed ( $t^{1/5}$ ) and dotted ( $t^{1/2}$ ) black lines.

the competition between two key mechanisms: (i) the evaporative heating of vortex dipoles that drives the system toward higher energy per vortex states and (ii) dissipative single vortex dynamics arising from the vortex ‘friction’, which is caused by the presence of non-condensate atoms. Ultimately, the stronger of these vortex heating and cooling effects determines the fate of the entire vortex system.

In experiments [24, 25, 49, 60], non-condensate atoms are always present. Our results imply that as long as sufficiently high condensate fraction is maintained, the qualitative results of the zero temperature Gross–Pitaevskii simulations remain valid also in finite temperature systems. However, high condensate temperatures introduce dissipative effects into the vortex dynamics, resulting in cooling of the vortex gas and an erosion of vortex clustering.

In future, it will be interesting to study the cross-over from the anomalous to the thermal fixed point behaviour in further detail and to explore its potential connections to the theory of dynamical phase transitions [61]. Furthermore, the long-time evolution of the system at the coldest condensate temperatures remains an open problem—does the system eventually revert to the Gaussian fixed point by annihilating all vortices? Or does the lifetime of the clusters approach infinity in the zero temperature limit? External forcing of a superfluid will inevitably lead to the heating of the condensate, which naturally leads to the question: is it possible to achieve driven steady state quantum turbulence, and if so, what are the properties of such a non-equilibrium system?

## Acknowledgements

We are grateful to Thomas Billam, Thomas Gasenzer, Kristian Helmerson and Shaun Johnstone for useful discussions.

**Funding information** We acknowledge financial support from the Australian Research Council via Discovery Programme Projects DP130102321 (T. S.), DP170104180 (T. S.), FT180100020 (T. S.). This research was also partially supported by the Australian Research Council Centre of Excellence in Future Low-Energy Electronics Technologies (project number CE170100039) and funded by the

Australian Government.

## References

- [1] A. N. Kolmogorov, *The local structure of turbulence in incompressible viscous fluid for very large Reynolds numbers*, In *Dokl. Akad. Nauk SSSR*, vol. 30, pp. 299–303 (1941).
- [2] R. H. Kraichnan, *Inertial Ranges in Two-Dimensional Turbulence*, *Physics of Fluids* **10**(7), 1417 (1967), doi:[10.1063/1.1762301](https://doi.org/10.1063/1.1762301).
- [3] G. K. Batchelor, *Computation of the Energy Spectrum in Homogeneous Two-Dimensional Turbulence*, *The Physics of Fluids* **12**(12), II (1969), doi:[10.1063/1.1692443](https://doi.org/10.1063/1.1692443).
- [4] C. F. Barenghi, L. Skrbek and K. R. Sreenivasan, *Introduction to quantum turbulence*, *Proceedings of the National Academy of Sciences* **111**(Supplement\_1), 4647 (2014), doi:[10.1073/pnas.1400033111](https://doi.org/10.1073/pnas.1400033111).
- [5] L. Skrbek and K. R. Sreenivasan, *Developed quantum turbulence and its decay*, *Physics of Fluids* **24**(1), 011301 (2012), doi:[10.1063/1.3678335](https://doi.org/10.1063/1.3678335).
- [6] M. Reeves, T. Billam, B. Anderson and A. Bradley, *Identifying a Superfluid Reynolds Number via Dynamical Similarity*, *Physical Review Letters* **114**(15), 155302 (2015), doi:[10.1103/PhysRevLett.114.155302](https://doi.org/10.1103/PhysRevLett.114.155302).
- [7] W. J. Kwon, J. H. Kim, S. W. Seo and Y. Shin, *Observation of von Kármán Vortex Street in an Atomic Superfluid Gas*, *Physical Review Letters* **117**(24), 245301 (2016), doi:[10.1103/PhysRevLett.117.245301](https://doi.org/10.1103/PhysRevLett.117.245301).
- [8] M. T. Reeves, T. P. Billam, X. Yu and A. S. Bradley, *Enstrophy Cascade in Decaying Two-Dimensional Quantum Turbulence*, *Physical Review Letters* **119**(18), 184502 (2017), doi:[10.1103/PhysRevLett.119.184502](https://doi.org/10.1103/PhysRevLett.119.184502).
- [9] J. Maurer and P. Tabeling, *Local investigation of superfluid turbulence*, *EPL (Europhysics Letters)* **43**(1), 29 (1998).
- [10] J. Salort, C. Baudet, B. Castaing, B. Chabaud, F. Daviaud, T. Didelot, P. Diribarne, B. Dubrulle, Y. Gagne, F. Gauthier, A. Girard, B. Hébral *et al.*, *Turbulent velocity spectra in superfluid flows*, *Physics of Fluids* **22**(12), 125102 (2010), doi:[10.1063/1.3504375](https://doi.org/10.1063/1.3504375).
- [11] R. Numasato, M. Tsubota and V. S. L'vov, *Direct energy cascade in two-dimensional compressible quantum turbulence*, *Physical Review A* **81**(6), 063630 (2010).
- [12] A. S. Bradley and B. P. Anderson, *Energy Spectra of Vortex Distributions in Two-Dimensional Quantum Turbulence*, *Physical Review X* **2**(4), 041001 (2012), doi:[10.1103/PhysRevX.2.041001](https://doi.org/10.1103/PhysRevX.2.041001).
- [13] M. T. Reeves, T. P. Billam, B. P. Anderson and A. S. Bradley, *Inverse Energy Cascade in Forced Two-Dimensional Quantum Turbulence*, *Physical Review Letters* **110**(10), 104501 (2013), doi:[10.1103/PhysRevLett.110.104501](https://doi.org/10.1103/PhysRevLett.110.104501).

- [14] T. Kusumura, H. Takeuchi and M. Tsubota, *Energy Spectrum of the Superfluid Velocity Made by Quantized Vortices in Two-Dimensional Quantum Turbulence*, Journal of Low Temperature Physics **171**(5-6), 563 (2013), doi:[10.1007/s10909-012-0827-9](https://doi.org/10.1007/s10909-012-0827-9).
- [15] T. P. Billam, M. T. Reeves, B. P. Anderson and A. S. Bradley, *Onsager-Kraichnan Condensation in Decaying Two-Dimensional Quantum Turbulence*, Physical Review Letters **112**(14), 145301 (2014).
- [16] T. P. Billam, M. T. Reeves and A. S. Bradley, *Spectral energy transport in two-dimensional quantum vortex dynamics*, Physical Review A **91**(2), 023615 (2015), doi:[10.1103/PhysRevA.91.023615](https://doi.org/10.1103/PhysRevA.91.023615).
- [17] U. Frisch, *Turbulence: The legacy of A. N. Kolmogorov*, Cambridge University Press (1995).
- [18] L. Onsager, *Statistical hydrodynamics*, Il Nuovo Cimento **6**, 279 (1949).
- [19] A. C. White, C. F. Barenghi and N. P. Proukakis, *Creation and characterization of vortex clusters in atomic Bose-Einstein condensates*, Physical Review A **86**(1), 013635 (2012), doi:[10.1103/PhysRevA.86.013635](https://doi.org/10.1103/PhysRevA.86.013635).
- [20] T. Simula, M. J. Davis and K. Helmerson, *Emergence of Order from Turbulence in an Isolated Planar Superfluid*, Physical Review Letters **113**(16), 165302 (2014), doi:[10.1103/PhysRevLett.113.165302](https://doi.org/10.1103/PhysRevLett.113.165302).
- [21] A. J. Groszek, T. P. Simula, D. M. Paganin and K. Helmerson, *Onsager vortex formation in Bose-Einstein condensates in two-dimensional power-law traps*, Physical Review A **93**(4), 043614 (2016), doi:[10.1103/PhysRevA.93.043614](https://doi.org/10.1103/PhysRevA.93.043614).
- [22] A. Skaugen and L. Angheluta, *Vortex clustering and universal scaling laws in two-dimensional quantum turbulence*, Physical Review E **93**(3), 032106 (2016), doi:[10.1103/PhysRevE.93.032106](https://doi.org/10.1103/PhysRevE.93.032106).
- [23] A. J. Groszek, M. J. Davis, D. M. Paganin, K. Helmerson and T. P. Simula, *Vortex Thermometry for Turbulent Two-Dimensional Fluids*, Physical Review Letters **120**(3), 034504 (2018), doi:[10.1103/PhysRevLett.120.034504](https://doi.org/10.1103/PhysRevLett.120.034504).
- [24] S. P. Johnstone, A. J. Groszek, P. T. Starkey, C. J. Billington, T. P. Simula and K. Helmerson, *Negative absolute temperatures of vortices in a two-dimensional superfluid*, arXiv:1801.06952 [cond-mat, physics:physics] (2018), ArXiv: 1801.06952.
- [25] G. Gauthier, M. T. Reeves, X. Yu, A. S. Bradley, M. Baker, T. A. Bell, H. Rubinsztein-Dunlop, M. J. Davis and T. W. Neely, *Negative-Temperature Onsager Vortex Clusters in a Quantum Fluid*, arXiv:1801.06951 [cond-mat, physics:physics] (2018), ArXiv: 1801.06951.
- [26] K. E. Wilson, Z. L. Newman, J. D. Lowney and B. P. Anderson, *In situ imaging of vortices in Bose-Einstein condensates*, Physical Review A **91**(2), 023621 (2015), doi:[10.1103/PhysRevA.91.023621](https://doi.org/10.1103/PhysRevA.91.023621).
- [27] G. Gauthier, I. Lenton, N. M. Parry, M. Baker, M. J. Davis, H. Rubinsztein-Dunlop and T. W. Neely, *Direct imaging of a digital-micromirror device for configurable microscopic optical potentials*, Optica **3**(10), 1136 (2016), doi:[10.1364/OPTICA.3.001136](https://doi.org/10.1364/OPTICA.3.001136).

- [28] A. Powis, S. Sammut and T. Simula, *Vortex Gyroscope Imaging of Planar Superfluids*, Physical Review Letters **113**(16), 165303 (2014), doi:[10.1103/PhysRevLett.113.165303](https://doi.org/10.1103/PhysRevLett.113.165303).
- [29] S. W. Seo, B. Ko, J. H. Kim and Y. Shin, *Observation of vortex-antivortex pairing in decaying 2d turbulence of a superfluid gas*, Scientific Reports **7**(1), 4587 (2017), doi:[10.1038/s41598-017-04122-9](https://doi.org/10.1038/s41598-017-04122-9).
- [30] M. J. Davis, R. J. Ballagh and K. Burnett, *Dynamics of thermal Bose fields in the classical limit*, Journal of Physics B: Atomic, Molecular and Optical Physics **34**(22), 4487 (2001), doi:[10.1088/0953-4075/34/22/316](https://doi.org/10.1088/0953-4075/34/22/316).
- [31] M. J. Davis, S. A. Morgan and K. Burnett, *Simulations of Bose Fields at Finite Temperature*, Physical Review Letters **87**(16), 160402 (2001), doi:[10.1103/PhysRevLett.87.160402](https://doi.org/10.1103/PhysRevLett.87.160402).
- [32] P. B. Blakie, A. S. Bradley, M. J. Davis, R. J. Ballagh and C. W. Gardiner, *Dynamics and statistical mechanics of ultra-cold Bose gases using c-field techniques*, Advances in Physics **57**(5), 363 (2008), doi:[10.1080/00018730802564254](https://doi.org/10.1080/00018730802564254).
- [33] C. W. Gardiner and M. J. Davis, *The stochastic Gross–Pitaevskii equation: II*, Journal of Physics B: Atomic, Molecular and Optical Physics **36**(23), 4731 (2003), doi:[10.1088/0953-4075/36/23/010](https://doi.org/10.1088/0953-4075/36/23/010).
- [34] T. P. Simula and P. B. Blakie, *Thermal Activation of Vortex–Antivortex Pairs in Quasi-Two-Dimensional Bose–Einstein Condensates*, Physical Review Letters **96**(2), 020404 (2006), doi:[10.1103/PhysRevLett.96.020404](https://doi.org/10.1103/PhysRevLett.96.020404).
- [35] R. N. Valani, A. J. Groszek and T. P. Simula, *Einstein–Bose condensation of Onsager vortices*, New Journal of Physics **20**(5), 053038 (2018), doi:[10.1088/1367-2630/aac0bb](https://doi.org/10.1088/1367-2630/aac0bb).
- [36] P. B. Blakie and M. J. Davis, *Projected Gross-Pitaevskii equation for harmonically confined Bose gases at finite temperature*, Physical Review A **72**(6), 063608 (2005), doi:[10.1103/PhysRevA.72.063608](https://doi.org/10.1103/PhysRevA.72.063608).
- [37] C. W. Gardiner, J. R. Anglin and T. I. A. Fudge, *The stochastic Gross-Pitaevskii equation*, Journal of Physics B: Atomic, Molecular and Optical Physics **35**(6), 1555 (2002), doi:[10.1088/0953-4075/35/6/310](https://doi.org/10.1088/0953-4075/35/6/310).
- [38] O. Penrose and L. Onsager, *Bose–Einstein Condensation and Liquid Helium*, Physical Review **104**(3), 576 (1956), doi:[10.1103/PhysRev.104.576](https://doi.org/10.1103/PhysRev.104.576).
- [39] C. J. Pethick and H. Smith, *Bose-Einstein condensation in dilute gases*, Cambridge University Press, second edn. (2008).
- [40] G. R. Dennis, J. J. Hope and M. T. Johnsson, *XMDS2: Fast, scalable simulation of coupled stochastic partial differential equations*, Computer Physics Communications **184**(1), 201 (2013), doi:[10.1016/j.cpc.2012.08.016](https://doi.org/10.1016/j.cpc.2012.08.016).
- [41] O. Bühler, *Statistical mechanics of strong and weak point vortices in a cylinder*, Physics of Fluids **14**(7), 2139 (2002), doi:[10.1063/1.1483305](https://doi.org/10.1063/1.1483305).
- [42] R. H. Kraichnan and D. Montgomery, *Two-dimensional turbulence*, Reports on Progress in Physics **43** (1980).

- [43] V. L. Berezinskii, *Destruction of long-range order in one-dimensional and two-dimensional systems having a continuous symmetry group I. Classical systems*, Soviet Journal of Experimental and Theoretical Physics **32**(3), 493 (1971).
- [44] V. L. Berezinskii, *Destruction of long-range order in one-dimensional and two-dimensional systems possessing a continuous symmetry group II. Quantum systems*, Soviet Journal of Experimental and Theoretical Physics **34**(3), 610 (1972).
- [45] J. M. Kosterlitz and D. J. Thouless, *Ordering, metastability and phase transitions in two-dimensional systems*, Journal of Physics C: Solid State Physics **6**(7), 1181 (1973), doi:[10.1088/0022-3719/6/7/010](https://doi.org/10.1088/0022-3719/6/7/010).
- [46] X. Yu, T. P. Billam, J. Nian, M. T. Reeves and A. S. Bradley, *Theory of the vortex-clustering transition in a confined two-dimensional quantum fluid*, Physical Review A **94**(2), 023602 (2016), doi:[10.1103/PhysRevA.94.023602](https://doi.org/10.1103/PhysRevA.94.023602).
- [47] J. Schole, B. Nowak and T. Gasenzer, *Critical dynamics of a two-dimensional superfluid near a nonthermal fixed point*, Physical Review A **86**(1), 013624 (2012), doi:[10.1103/PhysRevA.86.013624](https://doi.org/10.1103/PhysRevA.86.013624).
- [48] T. Kusumura, M. Tsubota and H. Takeuchi, *Formation of Quantum Turbulence from Dark Solitons in Atomic Bose-Einstein Condensates*, Journal of Physics: Conference Series **400**(1), 012038 (2012), doi:[10.1088/1742-6596/400/1/012038](https://doi.org/10.1088/1742-6596/400/1/012038).
- [49] W. J. Kwon, G. Moon, J. Choi, S. Seo and Y. Shin, *Relaxation of superfluid turbulence in highly oblate Bose-Einstein condensates*, Physical Review A **90**(6), 063627 (2014), doi:[10.1103/PhysRevA.90.063627](https://doi.org/10.1103/PhysRevA.90.063627).
- [50] G. W. Stagg, A. J. Allen, N. G. Parker and C. F. Barenghi, *Generation and decay of two-dimensional quantum turbulence in a trapped Bose-Einstein condensate*, Physical Review A **91**(1), 013612 (2015), doi:[10.1103/PhysRevA.91.013612](https://doi.org/10.1103/PhysRevA.91.013612).
- [51] A. Cidrim, F. E. A. dos Santos, L. Galantucci, V. S. Bagnato and C. F. Barenghi, *Controlled polarization of two-dimensional quantum turbulence in atomic Bose-Einstein condensates*, Physical Review A **93**(3), 033651 (2016), doi:[10.1103/PhysRevA.93.033651](https://doi.org/10.1103/PhysRevA.93.033651).
- [52] M. Karl and T. Gasenzer, *Strongly anomalous non-thermal fixed point in a quenched two-dimensional Bose gas*, New Journal of Physics **19**(9), 093014 (2017), doi:[10.1088/1367-2630/aa7eeb](https://doi.org/10.1088/1367-2630/aa7eeb).
- [53] A. W. Baggaley and C. F. Barenghi, *Decay of homogeneous two-dimensional quantum turbulence*, Physical Review A **97**(3), 033601 (2018), doi:[10.1103/PhysRevA.97.033601](https://doi.org/10.1103/PhysRevA.97.033601).
- [54] S. Erne, R. Bücke, T. Gasenzer, J. Berges and J. Schmiedmayer, *Universal dynamics in an isolated one-dimensional Bose gas far from equilibrium*, Nature **563**(7730), 225 (2018), doi:[10.1038/s41586-018-0667-0](https://doi.org/10.1038/s41586-018-0667-0).
- [55] M. Prüfer, P. Kunkel, H. Strobel, S. Lannig, D. Linnemann, C.-M. Schmied, J. Berges, T. Gasenzer and M. K. Oberthaler, *Observation of universal dynamics in a spinor Bose gas far from equilibrium*, Nature **563**(7730), 217 (2018), doi:[10.1038/s41586-018-0659-0](https://doi.org/10.1038/s41586-018-0659-0).

- [56] M. Karl, H. Cakir, J. C. Halimeh, M. K. Oberthaler, M. Kastner and T. Gasenzer, *Universal equilibrium scaling functions at short times after a quench*, Physical Review E **96**(2), 022110 (2017), doi:[10.1103/PhysRevE.96.022110](https://doi.org/10.1103/PhysRevE.96.022110).
- [57] I. Chantesana, A. P. Orioli and T. Gasenzer, *Kinetic theory of non-thermal fixed points in a Bose gas*, arXiv:1801.09490 [cond-mat, physics:hep-ph, physics:physics] (2018), ArXiv: 1801.09490.
- [58] A. J. Groszek, D. M. Paganin, K. Helmerson and T. P. Simula, *Motion of vortices in inhomogeneous Bose-Einstein condensates*, Physical Review A **97**(2), 023617 (2018), doi:[10.1103/PhysRevA.97.023617](https://doi.org/10.1103/PhysRevA.97.023617).
- [59] T. Simula, *Vortex mass in a superfluid*, Physical Review A **97**(2), 023609 (2018), doi:[10.1103/PhysRevA.97.023609](https://doi.org/10.1103/PhysRevA.97.023609).
- [60] T. W. Neely, A. S. Bradley, E. C. Samson, S. J. Rooney, E. M. Wright, K. J. H. Law, R. Carretero-González, P. G. Kevrekidis, M. J. Davis and B. P. Anderson, *Characteristics of Two-Dimensional Quantum Turbulence in a Compressible Superfluid*, Physical Review Letters **111**(23), 235301 (2013), doi:[10.1103/PhysRevLett.111.235301](https://doi.org/10.1103/PhysRevLett.111.235301).
- [61] M. Heyl, *Dynamical quantum phase transitions: a review*, Reports on Progress in Physics **81**(5), 054001 (2018), doi:[10.1088/1361-6633/aaaf9a](https://doi.org/10.1088/1361-6633/aaaf9a).